Electronic Decoherence Induced by Intramolecular Vibrational Motions in a Betaine Dye Molecule†

Hyonseok Hwang and Peter J. Rossky*

Institute for Theoretical Chemistry, Department of Chemistry and Biochemistry, University of Texas, Austin, Texas 78712-1167

Received: October 8, 2003; In Final Form: January 12, 2004

Electronic decoherence induced only by intramolecular vibrational motions is investigated in a betaine molecule, pyridinium *N*-phenoxide betaine [4-(1-pyridinio)phenolate], having 60 vibrational modes. The analysis is based on the nuclear overlap/phase function (NOPF) that appears in the electronic reduced density matrix. To do so, geometry optimizations and vibrational normal-mode analysis in the ground state and the first excited state are performed. Coherence dissipation times according to alternative approximations are obtained, including analysis of the role of frequency shifts and Duschinsky rotation. Geometry optimization reveals a large difference between the central torsional angles of the ground and the first excited state, with a tilted geometry of the pyridinium ring also observed in the first excited state. Nevertheless, the Duschinsky rotation matrix appears nearly diagonal with only a few considerable off-diagonal elements. We find that the low frequency torsional motion does not make any significant contribution to the decay of the NOPF. Frequency shifts have more effect on the decay of the NOPF than the Duschinsky rotation does, but the simplest spin-boson model alone describes coherence decay quite well. At times long compared to the main Gaussian decay, we also observe an exponential decay modulated by phase recurrence, but the exponential decay is dominant only for the last 10−20% of the relaxation. The calculated coherence dissipation time arising from intramolecular vibrational motions of 3.7 fs is much shorter than an estimate of the contribution to the decoherence time due to typical solvent molecules, indicating that nuclear motions in a solute molecule can have more influence on the total electronic decoherence than do solvent molecules even for a charge-transfer system such as the present case.

I. Introduction

Many chemical processes in condensed phases require using quantum mechanical methods. Among those processes are intra- and intermolecular electron transfer (ET) reactions,[1] proton-transfer reactions,[2] and electronic relaxation dynamics[3] of a solvated electron. In the case of many degrees of freedom, however, a fully quantum mechanical treatment is intractable because it is required to follow all degrees of freedom in configuration space. One method to address this difficulty is the use of mixed quantum-classical molecular dynamics (MQC-MD) methods where the subsystem degrees of freedom of interest (electrons or light particles) are described with quantum mechanics and the remaining bath degrees of freedom (nuclei or heavy particles) are described classically.[4−6] However, it has been appreciated that the classical description of bath degrees of freedom can have important and direct impact on observed rate processes.[7] In a full quantum description, subsystem coherence loss can occur due to the divergent evolution of nuclear states corresponding to alternative quantum states of the subsystem; this coherence loss is expected to occur very rapidly in condensed phases.[8−11] For example, the incomplete treatment of decoherence in MQC-MD methods introduces a large hydrogen isotope effect into the relaxation dynamics of the solvated electron, in contrast to experiment.[12]

Here we will emphasize the contributions to electronic decoherence that are associated with nuclear quantum effects. These contributions to electronic decoherence can be separately quantified for a given Hamiltonian model. Electronic pure dephasing, coherence loss associated with electronic energy gap fluctuations (diagonal coupling to nuclear coordinates), does appear in all MQC-MD methods, although the fluctuations in MQC methods are described completely classically.[13] The contribution to the decay of electronic coherences that is associated with nuclear quantum effects necessarily decreases with increasing temperature, as classical mechanics becomes increasingly accurate, whereas pure dephasing contributions increase with increasing temperature due to the increase in the magnitude of fluctuations.[11,14]

The understanding of decoherence is of importance in that it not only gives better insight into phenomena occurring in condensed phases but also provides a way to overcome the weakness of MQC-MD methods mentioned above. Of particular interest is the quantitative estimation of the contribution of nuclear quantum effects to the decoherence time because the implementation of the dissipative effects of decoherence into MQC-MD methods requires a reasonable estimation of the time.[15,16]

As mentioned above, decoherence gives rise to decay of off-diagonal elements in the reduced density matrix. An additional point of interest is the long-time behavior of that decay because it is associated with many spectroscopic phenomena such as zero-phonon line shapes in optical spectra.[17,18] Using a non-perturbative method, Skinner et al. showed that the decay in the long-time limit is exponential.[19−21] Reichman and Silbey

† Part of the special issue "Hans C. Andersen Festschrift".

10.1021/jp037031b CCC: $27.50
Published on Web 03/13/2004

used the ohmic spectral density in a two-level system to show that there is some deviation from the expected exponential behavior for experimentally accessible times in very low temperatures.[22]

One avenue to study decay of off-diagonal elements in the electronic reduced density matrix and to obtain an electronic decoherence time is by using a nuclear overlap/phase function (NOPF). The NOPF is the overlap between nuclear wave packets evolving on different electronic potential energy surfaces (PES). This function is responsible for the decay of off-diagonal elements.[23] Quantitative examination of the NOPF allows us to directly measure coherence time scales.[24−26] Therefore, evaluation of this function with a proper approximation can provide decoherence times for NA transition occurring in a condensed phase system.[8] For example, Prezhdo and Rossky used a Gaussian form for the NOPF, following from the earlier development by Neria and Nitzan,[24,25] to develop an approximate equation for the decoherence time, and applied the equation to obtain decoherence times for the relaxation of an excited solvated electron in water and heavy water.[8] Lockwood et al. have used molecular dynamics simulation to find a decoherence time for ET between metal ions in ruthenated azurin in water.[10]

Betaine dye molecules are well-known for their distinct absorption bands corresponding to solvent polarities. The absorption band is attributed to the large dipole moment change between the ground and the first excited state caused by intramolecular ET. Due to this intrinsic property, betaine molecules have long attracted significant experimental[27−34] and computational[35−38] attention. Using transient absorption spectroscopy, Barbara and co-workers[28−31] have studied intramolecular back ET rates occurring in the excited state of the betaine-30 molecule. Zong and McHale[32] focused on the effects of intramolecular vibrational modes as well as solvents on the relaxation following excitation in betaine-30 using resonance Raman spectroscopy. Among computational studies on that dye molecule, Mente and Maroncelli elucidated solvation dynamics on a molecular basis by carrying out Monte Carlo simulations of the betaine-30 dye molecule in various solvents.[36] Lobaugh and Rossky investigated the dynamics of the betaine-30 molecule after excitation to the first excited state and elucidated solvent and intramolecular effects on the absorption spectrum of betaine-30.[37,38]

In the present study, we focus on the quantitative description of this popular molecular probe. The simplest betaine, pyridinium *N*-phenoxide betaine [4-(1-pyridinio)phenolate], isolated in the gas phase, is investigated to examine electronic decoherence between the ground and the first excited state that is induced by intramolecular vibrational motions. Figure 1 shows this simplest betaine molecule, consisting of a pyridinium ring and a phenoxide ring, linked by an N−C band.

For most intramolecular vibrational motions, we will employ a harmonic PES, which has extensively been used for vibrational or vibronic spectrum calculations and NA transition rate calculations.[39−41] We include frequency shifts and Duschinsky rotation (mode mixing), which can play a role in vibrational motions.[42−46] This inclusion allows us to study the effects of frequency shifts and Duschinsky rotation on electronic decoherence. In general, a torsional motion cannot be described by a harmonic PES due to the softness and periodicity of that coordinate. In most methods related to a torsional motion, a periodic potential energy function for the torsional PES is sought, and the torsional motion is considered as a wave packet evolving on the potential energy function.[47−49] We follow this methodology here, and by doing so, we also study the effect of the torsional motion on decoherence.

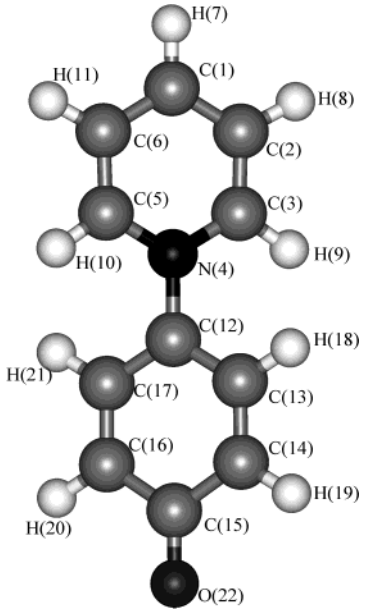

Figure 1. Molecular geometry and atom labelings of pyridinium *N*-phenoxide betaine [4-(1-pyridinio)phenolate].

We will investigate both the short-time and long-time behavior of the NOPF, which is directly related to the decay of off-diagonal elements in the reduced density matrix.[23] We will also use the NOPF to obtain intramolecular motion-induced decoherence times based on alternative approximations. Finally, comparing the decoherence times obtained here to estimated decoherence times due to solvent nuclear motions, we will be able to examine the relative contributions of nuclear motions from solute and solvent.

This work is organized as follows. In the following section, we present the theoretical methods to obtain displacements and frequencies for the ground and the first excited state as well as the Duschinsky rotation matrix. The detailed procedure to calculate the NOPF is given as well. In section III, the calculated results are shown and discussed. Finally, conclusions are made in section IV.

II. Theoretical Methods

We begin by considering the ground and the first excited state of the simplest betaine molecule in the gas phase. Of particular interest here is the influence of electronic decoherence on the NA transition from the first excited state to the ground state. Considering the ultrafast time scales of intramolecular vibrational motions, we make the reasonable and conventional[30] assumption that the initial state is the equilibrium geometry in the first excited state. We also use the low temperature limit for calculations, equivalent to assuming that the excited state vibrations are all in their ground state.

The Hamiltonian of the system composed of these two electronic states can then be expressed in terms of mass-weighted normal coordinates $\mathbf{Q} = \{Q_1, Q_2, ..., Q_{3N-6}\}$ where N is the number of atoms in the molecule

$$\hat{H} = |\mathrm{g}\rangle\hat{H}_\mathrm{g}\langle\mathrm{g}| + |\mathrm{e}\rangle\hat{H}_\mathrm{e}\langle\mathrm{e}| + \gamma^\dagger|\mathrm{e}\rangle\langle\mathrm{g}| + \gamma|\mathrm{g}\rangle\langle\mathrm{e}| \qquad (1)$$

where $|\mathrm{g}\rangle$ denotes the electronic ground state and $|\mathrm{e}\rangle$ the first excited state. γ is an electronic coupling matrix element, whereas $\hat{H}_\mathrm{g}$ and $\hat{H}_\mathrm{e}$ are the nuclear Hamiltonians on electronic surfaces $|\mathrm{g}\rangle$ and $|\mathrm{e}\rangle$, respectively

$$\hat{H}_g = \hat{T}(\dot{\mathbf{Q}}_g) + \hat{V}_g(\mathbf{Q}_g) \quad (2a)$$

$$\hat{H}_e = \hat{T}(\dot{\mathbf{Q}}_e) + \hat{V}_e(\mathbf{Q}_e) \quad (2b)$$

Here $\hat{T}$ and $\hat{V}$ are the kinetic and the potential energy operators, respectively.

The dynamics of an electronic subsystem can be expressed in terms of a reduced density matrix $\rho(t)$.[23,26] For our two-level system, we can write the matrix evolving from the initial conditions stated above as

$$\rho(t) = \begin{pmatrix} |c_e(t)|^2 & c_e(t)\, c_g^*(t)\, J^*(t) \\ c_e^*(t)\, c_g(t)\, J(t) & |c_g(t)|^2 \end{pmatrix} \quad (3)$$

where $c_e(t)$ and $c_g(t)$ are the amplitudes of electronic wave functions in the first excited and ground states, respectively. The NOPF, $J(t)$ in eq 3, is given as[8,24,26]

$$J(t) = \left\langle \Psi_e(0) \right| \exp\left[\frac{i}{\hbar}\hat{H}_e t\right] \exp\left[-\frac{i}{\hbar}\hat{H}_g t\right] \left| \Psi_e(0) \right\rangle \quad (4)$$

where $\Psi_e(0)$ is the initial nuclear wave function prepared in the equilibrium geometry of the first excited state. $J(t)$ is related by Fourier transformation to the emission spectrum in the Condon approximation;[8] spectra for this system are considered in detail in a separate paper.[14]

Up to this point, a general description for the NOPF has been provided. We now invoke some reasonable approximations for the calculation of the NOPF for intramolecular vibrational motions. First, harmonic PES are utilized for the vibrational motions other than the torsional motion. In many cases, the spin-boson model,[50] which only considers coordinate displacements in harmonic potentials, is sufficient to describe a system.[51] In general, however, frequency shifts and mixing of modes (Duschinsky rotation) must be taken into account to precisely explain the change of the vibrational normal modes accompanied by an electronic transition.[45,46] Frequency shifts occur due to force constant differences between two PES's, and Duschinsky rotation arises when two electronic states have different vibrational normal mode coordinate systems. We describe how we obtain frequency shifts and the Duschinsky rotation matrix in the following subsection. Due to the periodic torsional PES and the large difference between the optimized torsional angles of the two states (see below), the torsional PES is beyond a harmonic potential description. For the torsional motion, we use a method proposed by Seidner et al.[47] and used popularly by others.[48,49] This method will also be described in detail in the second subsection.

We now decompose the nuclear Hamiltonian in eq 1 into two parts[52]

$$\hat{H} = \hat{H}^{har} + \hat{H}^{tor} \quad (5)$$

where $\hat{H}^{har}$ means the Hamiltonian describing all the vibrational motions under the harmonic potential approximation and $\hat{H}^{tor}$ represents the Hamiltonian for the torsional motion. The torsional motion decouples from the other modes and can be treated separately if we assume

$$[\hat{H}^{har}, \hat{H}^{tor}] = 0 \quad (6)$$

This approximation is based on the time scale difference between slow torsional motions and other motions. Under this approximation, the NOPF from eq 4 can be factored into a product, which is given by

$$J(t) = J^{har}(t)\, J^{tor}(t) \quad (7)$$

where $J^{har}(t)$ is the NOPF corresponding to $\hat{H}^{har}$ and $J^{tor}(t)$ corresponding to $\hat{H}^{tor}$. The detailed expressions for $J^{har}(t)$ and $J^{tor}(t)$ as well as $\hat{H}^{har}$ and $\hat{H}^{tor}$ are provided next.

A. Harmonic Potential Approximation with Frequency Changes and Duschinsky Rotation. Here we consider $3N - 7$ vibrational degrees of freedom; the seventh degree of freedom excluded is the torsional degree of freedom. As mentioned above, the initial state is the first excited state and the final state is the ground state, and those two states are coupled through vibrational motions that are expressed by mass-weighted normal coordinates $\mathbf{Q} = \{Q_1, Q_2, ..., Q_{3N-7}\}$. The nuclear Hamiltonians in the two states, which are assumed to be harmonic, differ by frequency shifts and Duschinsky rotation as well as the displacement of the equilibrium nuclear positions. The Hamiltonian is then given by

$$\hat{H}^{har} = |g\rangle\hat{H}_g^{har}(\mathbf{Q}_g)\langle g| + |e\rangle\hat{H}_e^{har}(\mathbf{Q}_e)\langle e| + \gamma^{har}(|g\rangle\langle e| + |e\rangle\langle g|) \quad (8)$$

where γ^{har} is assumed to be real and static and

$$\hat{H}_g^{har}(\mathbf{Q}_g) = \frac{1}{2}\dot{\mathbf{Q}}_g^T\dot{\mathbf{Q}}_g + \frac{1}{2}\mathbf{Q}_g^T\Omega_g\mathbf{Q}_g \quad (9a)$$

$$\hat{H}_e^{har}(\mathbf{Q}_e) = \frac{1}{2}\dot{\mathbf{Q}}_e^T\dot{\mathbf{Q}}_e + \frac{1}{2}\mathbf{Q}_e^T\Omega_e\mathbf{Q}_e + \Delta G \quad (9b)$$

Here Ω_e and Ω_g are diagonalized frequency matrices in each state and ΔG is the potential energy minimum difference between two states. $\mathbf{Q}^T$ is the transpose of $\mathbf{Q}$.

To evaluate the integral of $J^{har}(t)$, we should express the coordinates of the ground state as functions of the coordinates of the first excited state. This can be accomplished by a linear combination[42,51,53]

$$\mathbf{Q}_g = \mathbf{D}\mathbf{Q}_e + \Delta\mathbf{Q} \quad (10)$$

where $\mathbf{D}$ means the Duschinsky rotation matrix and $\Delta\mathbf{Q}$ represents a displacement vector between the minima of the two states.

There are at least two methods to obtain $\mathbf{D}$ and $\Delta\mathbf{Q}$.[51,54] In one straightforward approach, geometry optimizations for each electronic state are performed independently.[54−56] But in an alternative method due to Lee et al,[51] the geometry optimization is only carried out for the initial electronic state, and the geometry of the final electronic state is estimated by projecting the Hessian matrix (force constant matrix) at the optimized geometry of the initial state. Due to the difference of the two methods, one obtains different frequencies, $\mathbf{D}$, and $\Delta\mathbf{Q}$ from each method. When we calculate reorganization energies associated with intramolecular vibrational coordinates using each method and compare those reorganization energies to experimental data,[30] the reorganization energy obtained from the straightforward method is unreasonably large whereas the energy from the other method is acceptable. This results from the relatively large displacements in the present case. We therefore adopt Lee et al.'s method[51] for our calculation.

Following ref 51, we first optimize the excited state and perform frequency analysis of that electronic state to obtain the Ω_e and $3N \times (3N - 7)$ transformation matrix $\mathbf{L}_e^{mx}$, which transforms mass-weighted Cartesian coordinates into normal coordinates. Next we calculate the Hessian matrix and the mass-weighted force vector (gradient) of the ground state at the

equilibrium position of the first excited state. The Duschinsky matrix can be evaluated with

$$\Omega_g{}^2 = \mathbf{D}(\mathbf{L}_e^{mx})^T \mathbf{K}_g^{mx} \mathbf{L}_e^{mx} \mathbf{D}^T \tag{11}$$

Here $\mathbf{K}_g^{mx}$ is the Hessian matrix of the ground state in Cartesian coordinates. In eq 11, $\Omega_g{}^2$ and $\mathbf{D}$ can be obtained simultaneously by diagonalizing $(\mathbf{L}_e^{mx})^T \mathbf{K}_g^{mx} \mathbf{L}_e^{mx}$ with the symmetry matrix eigenvalue (SME) method or the singular value decomposition (SVD) method.[57] The mass-weighted displacement vector $\Delta\mathbf{Q}$ is then calculated from

$$\Delta\mathbf{Q} = (\Omega_g{}^2)^{-1} \mathbf{D}(\mathbf{L}_e^{mx})^T \mathbf{F}_g^{mx} \tag{12}$$

where $\mathbf{F}_g^{mx}$ is the mass-weighted gradient of the ground state PES obtained at the equilibrium position of the first excited state. $\mathbf{F}_g^{mx}$ is expressed in terms of Cartesian coordinates.

To obtain $J^{har}(t)$, we will use the analytical finite temperature result; we obtain the low temperature result conveniently by evaluating the function at very low temperature. The thermally averaged NOPF for harmonic motions $\langle J^{har}(t)\rangle_T$ has an exact solution with the assistance of Kubo−Toyozawa formalism,[40,51,58]

$$\langle J^{har}(t)\rangle_T = \exp\left[-\frac{it}{\hbar}\Delta G - f_1(t) - f_2(t)\right] \tag{13}$$

where

$$f_1(t) = \Delta\mathbf{Q}^T \Theta_e (\Theta_e + \tilde{\Theta}_g)^{-1} \tilde{\Theta}_g \Delta\mathbf{Q} \tag{14}$$

and

$$f_2(t) = \frac{1}{2}\mathrm{Tr}\left[\ln\left\{\hbar^2\left(2\sinh\left(\frac{\beta\hbar\Omega_e}{2}\right)\right)^{-2} \Omega_e{}^{-1} \times \sinh((\beta p - it)\Omega_e)(\Theta_e + \tilde{\Theta}_g)(\Phi_e + \tilde{\Phi}_g)\Omega_g{}^{-1} \sinh(i\Omega_g t)\right\}\right] \tag{15}$$

Tr means trace and the matrices above are defined as

$$\Theta_e = \frac{1}{\hbar}\Omega_e \tanh\left\{\frac{(\beta\hbar - it)\Omega_e}{2}\right\} \tag{16a}$$

$$\Theta_g = \frac{1}{\hbar}\Omega_g \tanh\left\{\frac{i\Omega_g t}{2}\right\} \tag{16b}$$

$$\Phi_e = \frac{1}{\hbar}\Omega_e \coth\left\{\frac{(\beta\hbar - it)\Omega_e}{2}\right\} \tag{17a}$$

$$\Phi_g = \frac{1}{\hbar}\Omega_g \coth\left\{\frac{i\Omega_g t}{2}\right\}, \tag{17b}$$

$$\tilde{\Theta}_g = \mathbf{D}^T \Theta_g \mathbf{D} \tag{18a}$$

$$\tilde{\Phi}_g = \mathbf{D}^T \Phi_g \mathbf{D} \tag{18b}$$

and $\beta = 1/k_B T$.

In the case of the spin-boson model, $\mathbf{D}$ becomes the identity matrix and $\Omega_g = \Omega_e = \{\omega_1, \omega_2, ..., \omega_{3N-7}\}$. As a result, $f_2(t) = 0$ and $\langle J^{har}(t)\rangle_T$ is given as

$$\langle J_{SB}^{har}(t)\rangle_T = \exp\left[-\frac{it}{\hbar}\Delta G - \sum_j^{3N-7} S_j[\coth(\beta\hbar\omega_j/2)(1 - \cos(\omega_j t)) + i\sin(\omega_j t)]\right] \tag{19}$$

where S_j is a Huang−Rhys factor and defined as $S_j = {}^1/_2\Delta Q_j{}^2$.

B. Torsional Motion. As mentioned above, the central interring torsional motion is well beyond a harmonic potential description due to a large torsional angle difference between the optimized geometries of the ground and the first excited state and the periodic torsional PES. To examine the torsional motion properly, we explicitly calculate the periodic torsional potential energy function for the torsional motion of the electronic ground state. The torsional dynamics is then described as a wave packet evolving on the periodic PES. The dynamics of that mode is obtained by solving directly the time-dependent Schrödinger equation (TDSE).[47,48,49]

One usually approximates the Hamiltonian for a torsional motion as[47,48,49]

$$\hat{H}^{tor} = |g\rangle\hat{H}_g^{tor}(\theta)\langle g| + |e\rangle\hat{H}_e^{tor}(\theta)\langle e| + \gamma^{tor}(|g\rangle\langle e| + |e\rangle\langle g|) \tag{20}$$

where γ^{tor} is assumed to be real and static and

$$\hat{H}_g^{tor}(\theta) = -\frac{\hbar^2}{2I^{tor}}\frac{\partial^2}{\partial\theta^2} + V_g^{tor}(\theta) \tag{21a}$$

$$\hat{H}_e^{tor}(\theta) = -\frac{\hbar^2}{2I^{tor}}\frac{\partial^2}{\partial\theta^2} + V_e^{tor}(\theta) \tag{21b}$$

where θ is the torsional angle between the pyridinium ring and the phenoxide ring and I^{tor} is a reduced moment of inertia. $V_g^{tor}(\theta)$ and $V_e^{tor}(\theta)$ are the torsional PES's of each state.

The reduced moment of inertia I^{tor} for the torsional angle defined about the bond between N(4) atom and C(12) atom in Figure 1 is given as[49]

$$I^{tor} = \frac{I_{py} I_{ph}}{I_{py} + I_{ph}} \tag{22}$$

In eq 22, I_{py} is defined as

$$I_{py} = \sum_j m_j \mathbf{r}_j{}^2 \tag{23}$$

where j means any atom in pyridinium ring and $\mathbf{r}_j$ represents the distance between atom j and the torsional axis defined by the N(4)−C(12) central bond. In the same manner, I_{ph} is

$$I_{ph} = \sum_k m_k \mathbf{r}_k{}^2 \tag{24}$$

The initial nuclear wave function is in the equilibrium position of the first excited state. Under this assumption, the harmonic potential can be used for the first excited state PES and the $V_e^{tor}(\theta)$ is given as

$$V_e^{tor}(\theta) = \frac{1}{2} I^{tor} (\omega_e^{tor})^2 (\theta - \theta_0^e)^2 \tag{25}$$

where θ_0^e is the torsional angle at the equilibrium configuration of the first excited state.

The harmonic potential, however, cannot be applied to the ground state because the nuclear positions are far from the

equilibrium positions of the ground state. In this case, the explicit torsional PES for the ground state is necessary. In general, the PES for the torsional motion is given as[59]

$$V_g^{tor}(\theta) = \frac{1}{2}\sum_n V_n(1 - \cos\{n(\theta - \theta_0^g)\}) \qquad (26)$$

where θ_0^g is the torsional angle at the equilibrium configuration of the ground state and n is an integer. To obtain parameters for the ground state torsional PES, potential energies are calculated by varying the torsional angle θ and then fitting the energies as a function of θ.

Now $J^{tor}(t)$ can be written as

$$J^{tor}(t) = \langle \Psi_e^{tor}(t) | \Psi_g^{tor}(t) \rangle \qquad (27)$$

where $\Psi_e^{tor}(t)$ and $\Psi_g^{tor}(t)$ are obtained by solving the TDSE

$$i\hbar\frac{\partial}{\partial t}\Psi_e^{tor}(t) = \hat{H}_e^{tor}\Psi_e^{tor}(t) \qquad (28)$$

and

$$i\hbar\frac{\partial}{\partial t}\Psi_g^{tor}(t) = \hat{H}_g^{tor}\Psi_g^{tor}(t) \qquad (29)$$

When we follow Seidner et al.'s work,[47] standard fast Fourier transformation (FFT) techniques[60,61] are used to propagate the wave functions, and the overlap in eq 27 is integrated with respect to the torsional angle θ.[47−49]

III. Results and Discussion

A. Geometry Optimizations and Normal-Mode Analysis. Geometry optimizations and frequency analysis are performed with the GAUSSIAN 98 program.[62] The geometry optimization in the ground state is carried out at the Hartree−Fock level with a 6-31G* basis set. Configuration interaction singles (CIS) with the same basis set is used to optimize the first excited state. Frequencies in this paper are scaled with the factor of 0.91.[63] The geometry optimizations of the ground and the first excited state are performed without applying any symmetries at first, and then by applying C_2 symmetry for the ground and C_s for the first excited state. The torsional angle between the pyridinium ring and the phenoxide ring in the first excited state is held fixed at 90° under the C_s symmetry. Because we found that the electronic energies under the symmetries are not significantly different from those without symmetries, we have applied the symmetries in all of our calculations.

Figure 2 shows the optimized geometries of the ground state and the first excited state. The central bond lengths between N(4) and C(12) (see Figure 1) are 1.42 and 1.39 Å in the ground and the first excited state. The optimized torsional angle of 41.7° in the ground state is increased to 90° in the first excited state. This angle difference is attributed to the π to π^* transition, and this difference has already been observed by an ab initio calculation study.[64,65] In addition, a tilted geometry of the pyridinium ring is observed in the first excited state. The tilted geometry with the same angle of 12.2° has also been reported by the calculation of Hogiu et al.[33]

In Table 1, frequencies and dimensionless displacements of 60 vibrational modes of the ground and the first excited state are listed, respectively. Among those vibrational modes are 37 totally symmetric vibrational modes and the others are nontotally symmetric modes. Note that only totally symmetric vibrational modes have displacements.[45] The ground state frequencies are

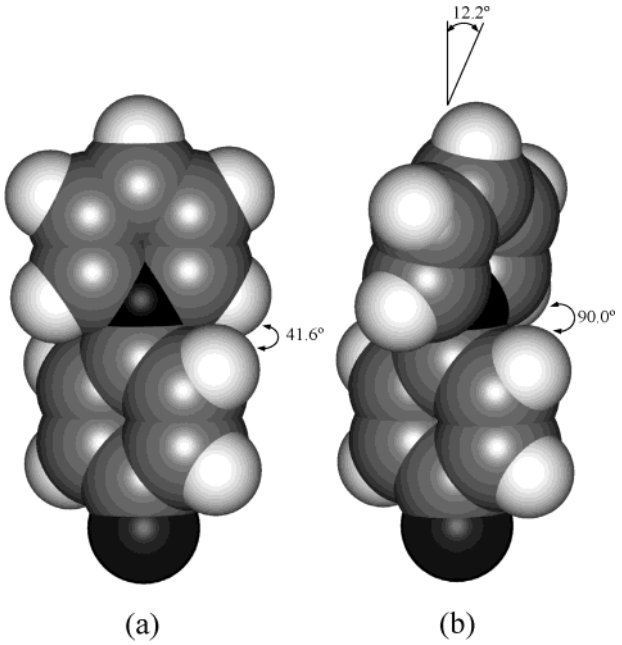

Figure 2. Optimized geometries of the ground (a) and first excited (b) states of the betaine molecule. The upper ring is the pyridinium and the lower the phenoxide ring. In (a), the torsional angle is 41.7°. In (b), the torsional angle is 90°, and the tilt angle of the pyridinium ring is 12.2°.

calculated by projecting the Hessian of the ground state on the normal coordinates of the first excited state and by diagonalizing the matrix. This calculation is performed by using eq 11. In this calculation, the Hessian matrix of the ground state is obtained at the equilibrium position of the first excited state. From our vibrational analysis, 56.5 cm^{-1} can be assigned to the frequency of the torsional mode in the ground state and 121.6 cm^{-1} in the first excited state. In the case of the inter-ring stretching mode, 294.4 cm^{-1} is assigned to the ground state and 280.0 cm^{-1} to the first excited state. Note that in Table 1, the displacement for the torsional mode is zero despite the large angle difference between the two optimized geometries. This is because the torsional mode in the first excited state is a nontotally symmetric mode, and due to the projection of the force constant matrix on the normal coordinates of the first excited state, the mode in the ground state also becomes a nontotally symmetric mode.

Hogiu et al.[33] also assigned some frequencies obtained from the Raman spectrum of betaine-30 to the torsional and the inter-ring stretching mode. In their analysis, they assigned 133 cm^{-1} to the torsional mode. The peak of 291 cm^{-1} was attributed to the inversion of the pyridinium nitrogen atom in their study, and 1209 cm^{-1} was assigned to the stretching mode. Because each corresponding ring in betaine-30 has effectively larger mass than the rings here due to phenyl groups attached to each ring in betaine-30, we believe that 1209 cm^{-1} is too high to be assigned to the inter-ring stretching mode. This issue is discussed by us further elsewhere.[66]

Figure 3 shows the contour map of the absolute values of the Duschinsky matrix elements $|D_{ij}|$ obtained from eq 11. Modes are numbered in order of increasing frequency. Although there are some off-diagonal elements in the low and middle frequency region, the map shows that the matrix is nearly diagonal, which suggests that Duschinsky matrix effect may not be large in this betaine molecule, and that a spin-boson model may be a good approximation. It is also evident that couplings occur largely between normal modes with similar

TABLE 1: 60 normal Mode Frequencies (cm^{-1}) and Displacements in the Ground and the First Excited States[a]

mode	ω_g	ω_e	ΔQ	mode	ω_g	ω_e	ΔQ	mode	ω_g	ω_e	ΔQ
1	69.5	28.1	−5.69	21	686.4	745.1	0.00	41	1480.6	1291.5	0.00
2	27.1	62.4	0.00	22	765.9	771.3	0.51	42	1327.2	1344.0	−0.59
3	56.5	121.6	0.00	23	768.4	810.9	0.00	43	1337.5	1370.0	0.00
4	154.0	170.5	0.00	24	838.9	876.7	0.00	44	1452.5	1427.2	0.03
5	282.6	201.5	1.56	25	936.3	953.1	0.28	45	1436.2	1447.7	−0.30
6	294.4	280.0	0.21	26	1025.9	969.0	0.00	46	1477.6	1478.4	0.29
7	369.2	352.0	0.00	27	949.4	969.2	−0.54	47	1522.8	1522.7	0.00
8	512.1	387.5	−0.36	28	1047.3	972.7	0.19	48	1528.0	1535.8	0.06
9	402.6	425.5	0.00	29	1006.6	999.4	0.36	49	1622.7	1620.2	0.02
10	410.0	434.9	0.00	30	1018.6	1008.2	−1.01	50	1670.2	1666.6	−0.99
11	435.7	457.0	−0.75	31	966.6	1018.7	0.00	51	1748.3	1746.3	0.30
12	556.5	538.3	0.19	32	960.8	1020.8	0.00	52	3092.9	3087.0	0.05
13	466.1	544.0	0.00	33	1155.1	1031.4	0.00	53	3094.6	3089.1	0.00
14	616.0	594.8	0.06	34	1115.2	1081.7	0.00	54	3076.7	3102.3	0.06
15	683.7	631.1	−0.39	35	1061.5	1097.1	0.00	55	3074.8	3102.8	0.00
16	620.1	635.3	0.00	36	1145.5	1163.1	−0.16	56	3104.3	3119.7	−0.04
17	804.7	658.3	0.08	37	1201.2	1206.5	0.70	57	3107.0	3121.4	0.06
18	699.4	692.2	0.39	38	1266.3	1252.0	−0.03	58	3145.5	3128.4	0.02
19	1000.7	720.8	−0.05	39	901.7	1261.8	0.00	59	3179.7	3154.4	0.00
20	874.1	737.2	0.00	40	1172.1	1285.0	0.03	60	3181.5	3158.7	0.06

[a] Configuration interaction singles (CIS) with 6-31G* is used to perform a geometry optimization for the first excited state. The frequencies of the ground state are obtained at the optimized geometry of the first excited state by diagonalizing the force constant matrix (Hessian matrix) of the ground state. Calculation for the force constant matrix is performed at the Hartree−Fock level with 6-31G*. The frequency scaling factor is 0.91, and displacements are unitless. See text.

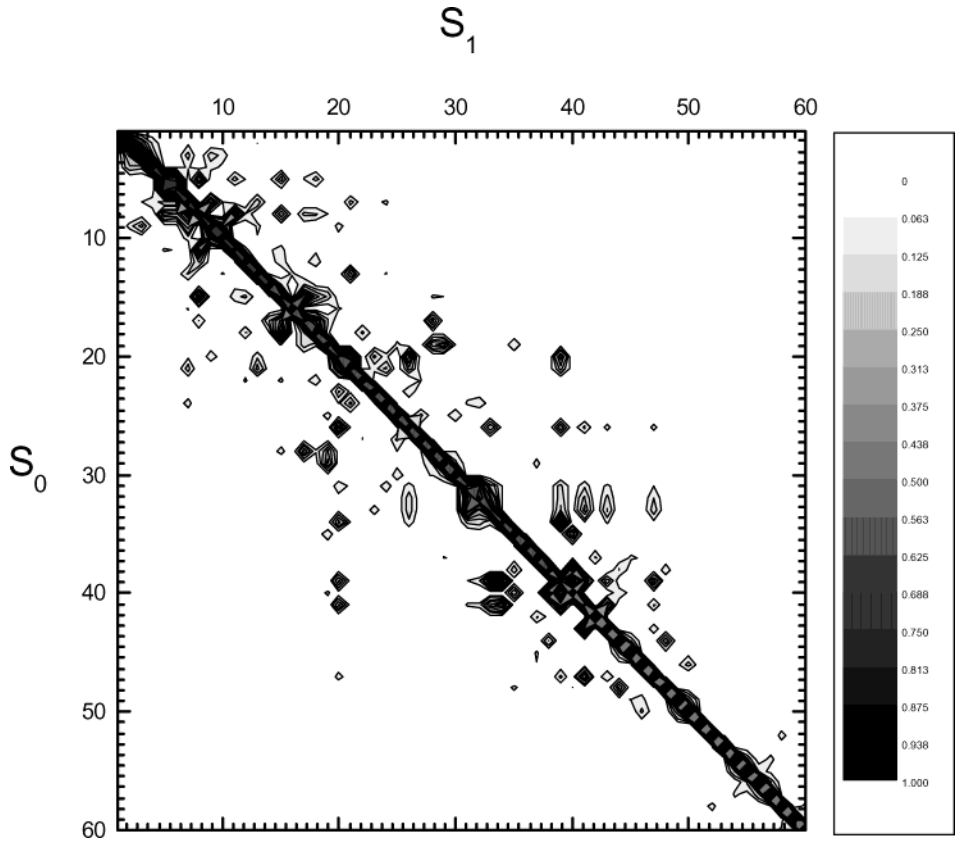

Figure 3. Duschinsky matrix elements between the ground (S_0) and the first excited (S_1) states. To see solely coupling strengths, absolute values of the elements are shown, namely, $|D_{ij}|$. The numbering is the same as in Table 1.

frequencies, and there are more couplings at low frequency than at middle or high frequencies. It is also seen that the nine C−H stretching modes of over 3000 cm^{-1} are not coupled to other modes at low or middle frequencies.

B. Nuclear Overlap/Phase Function, *J*(*t*). Figure 4 compares the decays of $|J^{har}(t)|$ and $|J^{tor}(t)|$ using eqs 13 and 27, respectively. In all the calculations of the desired NOPF, we obtain the low temperature limit conveniently simply by fixing the temperature at 8 K. At a temperature of 8 K, each normal mode, including the torsional mode, stays at its vibrational ground state in the first excited state. We note that for the treatment of the torsional dynamics, the moment of inertia (eq 22) and PES used are for the molecule lacking the 12.2° ring tilt (see Figure 2b), as in the ground state (Figure 2a). Figure 4 shows that the decay of $|J^{tor}(t)|$ is much slower than that of $|J^{har}(t)|$. The effect of the torsional motion on the electronic decoherence is therefore, as expected, insignificant when compared with the other vibrational modes.

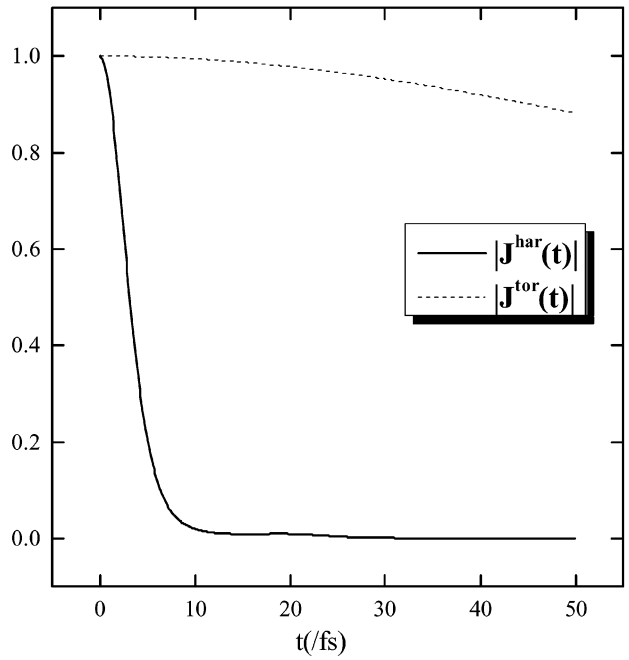

Figure 4. Comparison between $|J^{har}(t)|$ and $|J^{tor}(t)|$. The temperature is held at 8 K to satisfy the low temperature limit.

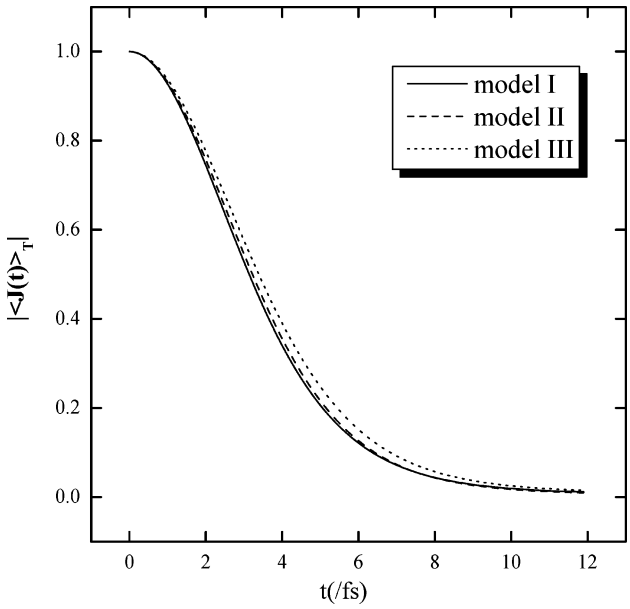

Figure 5. Comparison among several models for $|J(t)|$. Model I includes Duschinsky rotation as well as frequency shifts and displacements. In model II, Duschinsky rotation is not considered. In model III (spin-boson model), only displacements are taken into account. The temperature is the same as in Figure 4.

In Figure 5, we show alternative model descriptions of $|J^{har}(t)|$. Model I includes the effect of Duschinsky rotation as well as frequency shifts and displacements. Though frequency shifts and displacements are considered in model II, model III accounts solely for the effect of displacements (spin-boson model). As is evident from Figure 5, model II is somewhat different from model III, the differences originating from frequency shifts in the model II. A comparison between model I and model II shows that Duschinsky rotation has a very minor effect. On the basis of these observations, in our molecular system, frequency shifts introduce larger deviations from the spin-boson model than the Duschinsky rotation does. However, the differences among those three models are not large. Lee et al.[51] studied an ET reaction between the tryptophan cation radical and tyrosine, comparing reaction rates from those three models. Their results also reflected that both frequency shifts and Duschinsky rotation produced only a minor effect. Although these studies remain quite limited, and the generality is not established, these two detailed studies show that reasonable results can be obtained when a spin-boson model for complex polyatomic systems is used without further modifications such as frequency shifts or Duschinsky rotation.

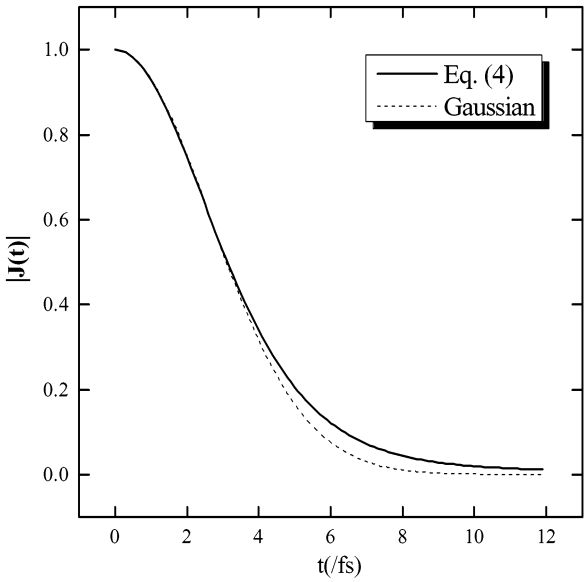

Figure 6. Comparison between $|J(t)|$ and $|J^{ga}(t)|$. The calculation for $|J^{ga}(t)|$ is based on eq 30. Frequency shifts and Duschinsky rotation are included.

Prezhdo and Rossky[8,67] used the frozen Gaussian approximation (FGA) to derive decoherence times in the short-time limit. The resulting thermally averaged NOPF $|\langle J(t)\rangle_T|$ has the form

$$|\langle J^{ga}(t)\rangle_T| \approx \exp\left[-\frac{1}{2}\frac{t^2}{(\tau_D^{ga})^2}\right] \tag{30}$$

The form of eq 30 implies

$$\tau_D^{ga} = \left[-\left\{\frac{d^2}{dt^2}\ln\left|\langle J(t)\rangle_T\right|\right\}_{t=0}\right]^{-1/2} \tag{31}$$

Figure 6 shows the comparison between the $|J(t)|$ based on eq 4 and the short-time Gaussian form of $|J(t)|$ based on eq 30. The approximation is made in the short-time regime, and the approximation is excellent up to 3 fs. It can be seen, however, that the deviation at longer times is not large. Equation 30 is also used to obtain an electronic decoherence time τ_D^{ga}, and the estimated value of τ_D^{ga} by the intramolecular vibrational modes is 2.64 fs. It is interesting to note that Lockwood et al. found that a corresponding decoherence time occurring in a solvated ET protein is 2.4 fs, with the protein alone accounting for a value of 4 fs, a quite comparable value.[11]

Now we investigate the longer time behavior of the NOPF. One phenomenon resulting from the finite number of normal modes in the calculation of the NOPF is phase recurrence, which means that formally the NOPF does not decay completely.[22,68,69] Figure 7a clearly shows phase recurrence. The first recurrence is associated with normal modes having higher frequencies and larger displacements. Table 1 shows that the 50th normal mode, of frequency around 1670 cm^{-1}, has a large displacement. The

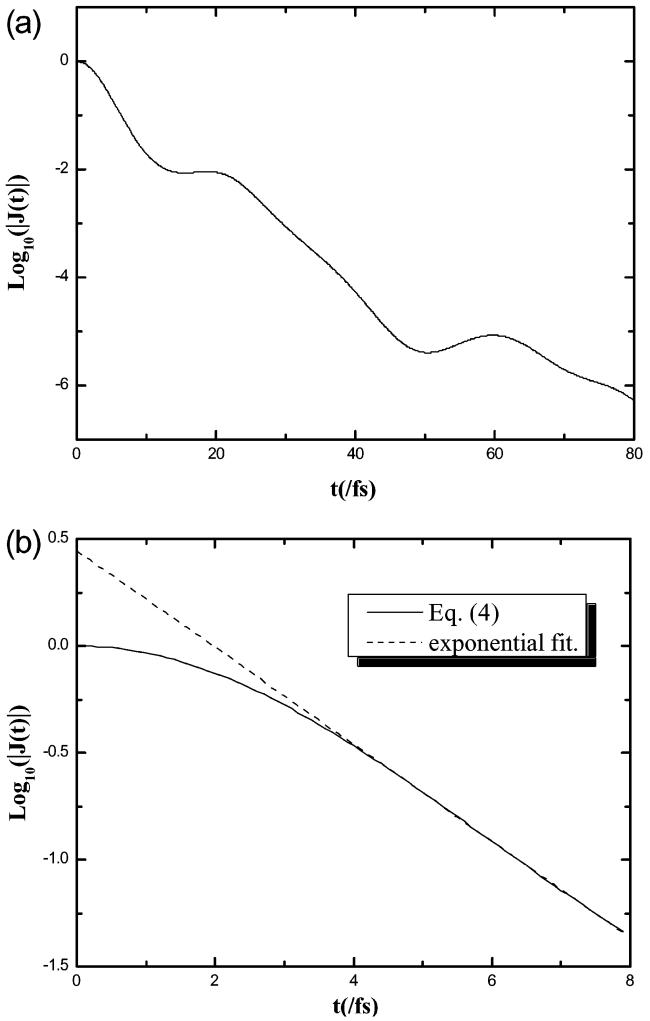

Figure 7. (a) Long-time behavior of $|J(t)|$. Phase recurrence is seen at around 20 fs. (b) Comparison between $|J(t)|$ and $|J^{exp}(t)|$. The calculation for $|J^{exp}(t)|$ is based on eq 32. Frequency shifts and Duschinsky rotation are included.

time scale of the first phase recurrence occurring at around 20 fs corresponds to this normal mode.

We noted earlier that theoretical considerations[19−22] imply exponential decay at long times. Even in this 60 mode system, we see in Figure 7a that decay beyond 5−10 fs is roughly exponential. From Figure 7b, we can see that an exponential-like decay apparently begins transiently at around 4.7 fs. When we use an exponential fitting function, for this time regime

$$|J^{exp}(t)| \approx \exp\left[-\frac{t}{\tau_d^{exp}}\right] \tag{32}$$

the τ_d^{exp} is estimated as approximately 1.91 fs. However, comparing the exponential decay with the Gaussian (Figure 6), we observe that the initial Gaussian decay is dominant. The roughly exponential decay characterizes only the last about 25%, and the characteristic time scale is comparable.

Now we consider why the exponential decay appears transiently at short times and is less dominant than the initial Gaussian decay in this system. Because the contributions of the torsional motion, frequency shifts, and Duschinsky rotation to the decay of the NOPF is not large, for analysis we can use a second-order truncation in the cumulant expansion of $|\langle J(t)\rangle_T|$ as a reasonable approximation for the harmonic vibrational motions. Then the result is given as[26,70]

$$|\langle J(t)\rangle_T| \approx \exp\left[-\frac{\langle(\delta\hat{U})^2\rangle_T}{\hbar^2}\int_0^t dt_2\int_0^{t_2} dt_1\ \mathrm{Re}\{C(t_1)\}\right] \tag{33}$$

Here the normalized energy gap fluctuation autocorrelation function $C(t)$ is defined as

$$C(t) = \frac{\langle\delta\hat{U}(t)\cdot\delta\hat{U}(0)\rangle_T}{\langle\delta\hat{U}(0)\cdot\delta\hat{U}(0)\rangle_T} \tag{34}$$

where $\delta\hat{U}(t)$ is defined as

$$\delta\hat{U}(t) = \Delta\hat{H}_{ge}(t) - \langle\Delta\hat{H}_{ge}\rangle_T \tag{35}$$

and $\Delta\hat{H}_{ge}$ is

$$\Delta\hat{H}_{ge} = \hat{H}_g - \hat{H}_e \tag{36}$$

When the normalized $C(t)$ decays completely before a typical correlation time of τ_c, for times $t \gg \tau_c$, eq 33 can be written as[26,71,72]

$$|\langle J(t)\rangle_T| \approx \exp\left[-\frac{\langle(\delta\hat{U})^2\rangle_T}{\hbar^2}Mt\right] \tag{37}$$

where M is defined as

$$M = \int_0^\infty dt_1\ \mathrm{Re}\{C(t_1)\} \tag{38}$$

From eq 37, we see the exponential decay of $|\langle J(t)\rangle_T|$. As a consequence, the conditions for the true exponential decay of $|\langle J(t)\rangle_T|$ are the complete relaxation (or decay) of $\mathrm{Re}\{C(t)\}$ before a typical correlation time, and faster decay of $\mathrm{Re}\{C(t)\}$ than $|\langle J(t)\rangle_T|$.

We plot the $\mathrm{Re}\{C(t)\}$ along with the $|\langle J(t)\rangle_T|$ in Figure 8 in the low temperature limit. It is clear that the decay of $\mathrm{Re}\{C(t)\}$ is actually slower than that of $|J(t)|$ until around 4.8 fs. (In addition, of course $\mathrm{Re}\{C(t)\}$ never decays completely due to the finite number of normal modes.) Hence, over the short time that most of the decay occurs, one has clearly not reached the exponential limit. The slower decay of $\mathrm{Re}\{C(t)\}$ in Figure 8 also explains the dominance of the initial Gaussian decay. When $\mathrm{Re}\{C(t)\}$ decays slowly, we can use $\mathrm{Re}\{C(t)\} \approx \mathrm{Re}\{C(0)\}$, and then $|\langle J(t)\rangle_T|$ can be approximated as

$$|\langle J(t)\rangle_T| \approx \exp\left[-\frac{\langle(\delta\hat{U})^2\rangle_T}{2\hbar^2}\mathrm{Re}\{C(0)\}t^2\right] \tag{39}$$

We also see from Figure 8 that the small time interval for the apparent exponential decay accords with the time interval where $\mathrm{Re}\{C(t)\}$ has small values; the conditions for the exponential decay are approximately and temporarily satisfied in such time regions. It is worth noting here that the expressions for $J(t)$ just above make clear that the decay seen here at low temperature is a quantum nuclear effect, because $\delta\hat{U}$ would be vanishingly small classically in the present case.

Electronic coherence dissipation times can be defined perhaps most conventionally by

$$\tau_d = \int_0^\infty dt\ |J(t)| \tag{40}$$

Using $|J^{ga}(t)|$ as the integrated function in eq 40, we define the resulting short-time approximate coherence dissipation time as τ_d^{STA}. We present various comparable coherence dissipation

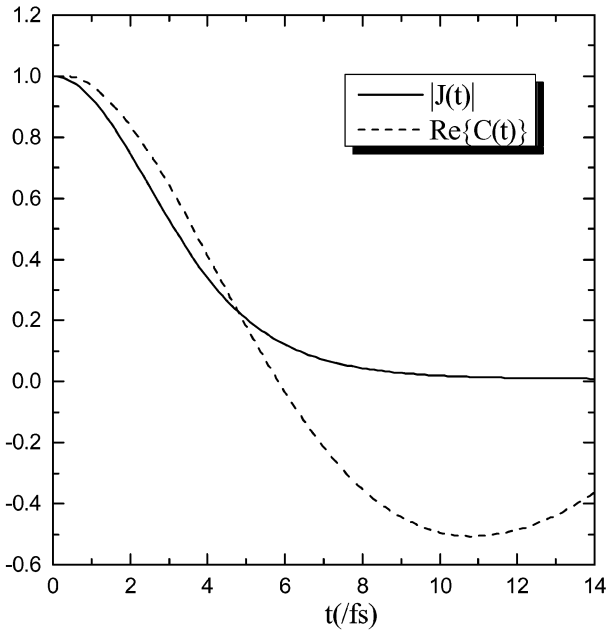

Figure 8. Decays of $|J(t)|$ and $\mathrm{Re}\{C(t)\}$. Frequency shifts and Duschinsky rotation are included.

TABLE 2: Various Electronic Decoherence Times[a]

	τ_D^{ga}	τ_d^{STA}	τ_d^{TI}	τ_d^{exp}
model I[b]	2.64	3.31	3.67	1.91
model II	2.71	3.40	3.72	1.85
model III	2.78	3.48	4.10	2.03

[a] Temperature is fixed at 8 K for the calculation of all τ_D's. Below are the definitions of the τ_D's:

$$\tau_D^{ga} \equiv -\frac{d^2}{dt^2}|\langle J(t)\rangle_T|_{t=0} \qquad \tau_d^{STA} \equiv \int dt \exp\left[-\frac{t^2}{2(\tau_D^{ga})^2}\right] = \sqrt{\frac{\pi}{2}}\tau_D^{ga}$$

$$\tau_d^{TI} \equiv \int dt\, |\langle J(t)\rangle_T| \qquad \tau_d^{exp} \equiv \left[-\left\{\frac{d}{dt}\ln\left|\langle J(t)\rangle_T\right|\right\}_{t=t_0}\right]^{-1}$$

[b] Definitions for models are the same as in Figure 5. See text. [c] In principle, τ_d^{exp} should be calculated at $t = \infty$, but due to the phase recurrence, τ_d^{exp} is calculated at $t = t_0$. Here t_0 is the time where the exponential decay is most prominent. See text.

times in Table 2. Table 2 shows that as the effects of frequency shifts and Duschinsky rotation are included (from model III to model I), the decoherence times become shorter. This is a reasonable result because nontotally symmetric modes can now participate in the decay of the NOPF through frequency shifts and Duschinsky rotation. However, note an exception in τ_d^{exp}, which is only a local decay rate.

We next consider solvent effects. Prezhdo and Rossky[67] proposed a relationship between the electronic decoherence time scale and the energy gap fluctuation time scale in the high temperature limit and estimated electronic decoherence times τ_D induced by only solvent molecules in several systems. In their study, decoherence times have been estimated as 4.5 fs for the first excited state of the hydrated electron in water, and to be 49 fs for the betaine-30 molecule in acetonitrile. If we assume that the vibrational coupling between the nuclei of a solute molecule and those of solvent molecules is small enough to be neglected and that the short-time approximation is valid, the total decoherence time τ_D^{tot} can be decomposed into

$$\left(\frac{1}{\tau_D^{tot}}\right)^2 \approx \left(\frac{1}{\tau_D^{solut}}\right)^2 + \left(\frac{1}{\tau_D^{solv}}\right)^2 \qquad (41)$$

where τ_D^{solut} stands for the decoherence time induced by the nuclei of the solute, and τ_D^{solv} the time induced by the solvent molecules.

Taking into account that a betaine-30 molecule has a larger number of normal modes than the simplest betaine, it is a reasonable speculation that the electronic decoherence time by intramolecular vibrational motions in a betaine-30 should be no longer than 2.64 fs, which is the decoherence time in the present simple betaine. If we use the time 2.64 fs for the τ_D^{solut} and 49 fs for the τ_D^{solv} in a betaine-30/acetonitrile system in eq 41, we obtain the expected 2.64 fs for the total electronic decoherence time in the betaine-30/acetonitrile system. The total is essentially the same as the decoherence time due to the intramolecular vibrational modes, implying that the nuclear motions of a charge-transfer polyatomic solute molecule such as a betaine molecule have far more effect on the decoherence time than the nuclear motions of solvent molecules even in condensed phases.

IV. Concluding Remarks

We have carried out geometry optimization and vibrational normal-mode analysis for the ground and the first excited states in a simple betaine dye molecule. In our study, the most prominent difference between geometries of the two electronic states was the torsional angle, which is attributed to the π to π^* transition. We have also shown that the frequencies of the torsional mode in the ground and the first excited state lie in the low frequency region, and the torsional mode is a nontotally symmetric mode. The inter-ring stretching mode frequencies in each state are not high due to the large masses of both rings. The Duschinsky matrix obtained is nearly diagonal, which suggests that Duschinsky rotation effects on electronic decoherence in this betaine molecule should not be large.

By using the nuclear overlap/phase function, we investigated electronic decoherence caused by quantized intramolecular vibrational motions in the molecule. In our study, contributions to the decay of the NOPF come from the harmonic vibrational motions, and the torsional motion is too slow to make a significant contribution to the decay. Frequency shifts have more influence on the decay of that function than Duschinsky rotation, but the deviation from the simple spin-boson model due to frequency shifts is also relatively small.

At longer times, we observed a transient of roughly exponential decay followed by superimposed phase recurrence in the decay of the NOPF. This phase recurrence occurred due to the finite number of normal modes (60). Compared with the initial Gaussian decay, the exponential decay was not dominant. This was explained by demonstrating that the condition for the exponential decay, i.e., fast and complete decay of the normalized energy gap fluctuation autocorrelation function, did not apply here.

Through a short-time (or Gaussian) approximation, we obtained an electronic coherence dissipation time of 3.3 fs from the intramolecular vibrational motions in the betaine molecule whereas an accurate calculation yields the similar 3.7 fs. Coherence dissipation times obtained with different approximations did not deviate significantly from each other. On the basis of those times, we find that electronic decoherence by intramolecular vibrational motions occurs on an ultrafast time scale. The ultrafast coherence loss time due to intramolecular vibrational motions suggests that the nuclear motions of polyatomic solute molecules such as a betaine dye can have much greater effect on the total electronic coherence loss than polar solvent molecules do. Correspondingly, one concludes that to implement

decoherence into an MQC-MD simulation on a polyatomic solute molecule in condensed phases, the incorporation of the decoherence effect from the solute molecule is critical, and it may be sufficient to capture the most important nuclear quantum effects.

Acknowledgment. We thank Dr. Kim F. Wong for stimulating discussions. We are also grateful to Dr. Sandro R. P. da Rocha for helpful comments on the manuscript. This work was supported by a grant from the National Science Foundation (CHE- 0134775) and by the R. A. Welch Foundation.

References and Notes

(1) Bolton, J. R.; Mataga, N.; MeLendon, G. In *Electron Transfer in Inorganic, Organic, and Biological Systems*; Bolton, J. R., Mataga, N., MeLendon, G., Eds.; American Chemical Society: Washington, DC, 1991.
(2) Link, T. A. In *Electron and Proton Transfer in Chemistry and Biology*; Muller, A., Ratajczaks, H., Junge, W., Diemann, E., Eds.; Elsevier: Amsterdam, 1992.
(3) Wong, K. F.; Rossky, P. J. *J. Phys. Chem. A* **2001**, *105*, 2546.
(4) Ehrenfest, P. *Z. Phys.* **1927**, *45*, 455.
(5) Tully, J. C. *J. Chem. Phys.* **1990**, *93*, 1061.
(6) Webster, F. A.; Rossky, P. J.; Friesner, R. A. *Comput. Phys. Commun.* **1991**, *63*, 494.
(7) Bittner, E. R.; Rossky, P. J. *J. Chem. Phys.* **1995**, *103*, 8130.
(8) Prezhdo, O.; Rossky, P. J. *J. Chem. Phys.* **1997**, *107*, 5863.
(9) Wynne, K.; Hochstrasser, R. M. *Adv. Chem. Phys.* **1997**, *107*, 263.
(10) Lockwood, D. M.; Cheng, Y.-K.; Rossky, P. J. *Chem. Phys. Lett.* **2001**, *345*, 159.
(11) Lockwood, D. M.; Hwang, H.; Rossky, P. J. *Chem. Phys.* **2001**, *268*, 285.
(12) Schwartz, B. J.; Rossky, P. J. *J. Chem. Phys.* **1996**, *105*, 6997.
(13) Rossky, P. J. In *Classical and Quantum Dynamics in Condensed Phase Simulations*; Berne, B. J., Ciccotti, G., Coker, D., Eds.; World Scientific: Singapore, 1997.
(14) Hwang, H.; Rossky, P. J. To be published.
(15) Wong, K. F.; Rossky, P. J. *J. Chem. Phys.* **2002**, *116*, 8418.
(16) Wong, K. F.; Rossky, P. J. *J. Chem. Phys.* **2002**, *116*, 8429.
(17) Maradudin, R. A. *Solid State Phys.* **1966**, *18*, 273.
(18) Skinner, J. L.; Hsu, D. *Adv. Chem. Phys.* **1986**, *65*, 1.
(19) Skinner, J. L. *J. Chem. Phys.* **1982**, *77*, 3398.
(20) Hsu, D.; Skinner, J. L. *J. Chem. Phys.* **1984**, *81*, 1604.
(21) Skinner, J. L.; Hsu, D. *J. Phys. Chem.* **1986**, *90*, 4931.
(22) Reichman, D.; Silbey, R. *J. Chem. Phys.* **1996**, *105*, 10500.
(23) Simonius, M. *Phys. Rev. Lett.* **1978**, *40*, 980.
(24) Neria, E.; Nitzan, A. *Phys. Rev. Lett.* **1993**, *67*, 1011.
(25) Neria, E.; Nitzan, A. *J. Chem. Phys.* **1993**, *99*, 1109.
(26) Mukamel, S. *Principles of Nonlinear Optical Spectroscopy*; Oxford University Press: Oxford, U.K., 1995.
(27) Reichardt, C. *Angew. Chem., Int. Ed. Engl.* **1979**, *18*, 98.
(28) Åkesson, E.; Walker, G. C.; Barbara, P. F. *J. Chem. Phys.* **1991**, *95*, 4188.
(29) Barbara, P. F.; Walker, G. C.; Smith, T. P. *Science* **1992**, *256*, 975.
(30) Walker, G. C.; Åkesson, E.; Johnson, A. E.; Levinger, N. E.; Barbara, P. F. *J. Phys. Chem.* **1992**, *96*, 3728.
(31) Reid, P. J.; Barbara, P. F. *J. Phys. Chem.* **1995**, *99*, 3554.
(32) Zong, Y.; McHale, J. L. *J. Chem. Phys.* **1997**, *106*, 4963.
(33) Hogiu, S.; Dreyer, J.; Pfeiffer, M.; Brzezinka, K.-W.; Werncke, W. *J. Raman Spectrosc.* **2000**, *31*, 797.
(34) Kovalenko, S. A.; Eilers-König, N.; Senyushkina, T. A.; Ernsting, N. P. *J. Phys. Chem. A* **2001**, *105*, 4834.
(35) Bartkowiak, W. L. Lipiński, *J. Phys. Chem. A* **1998**, *102*, 5236.
(36) Mente, S. R.; Maroncelli, M. *J. Phys. Chem. B* **1999**, *103*, 7704.
(37) Lobaugh, J.; Rossky, P. J. *J. Phys. Chem. A* **1999**, *103*, 9432.
(38) Lobaugh, J.; Rossky, P. J. *J. Phys. Chem. A* **2000**, *104*, 899.
(39) Wilson, J. E. B.; Decius, J. C.; Cross, P. C. *Molecular Vibrations*; McGraw-Hill: New York, 1955.
(40) Kubo, R.; Toyozawa, Y. *Prog. Theor. Phys.* **1955**, *13*, 160.
(41) Levine, I. N. *Molecular Spectroscopy*; John Wiley & Sons: New York, 1975.
(42) Sharp, T. E.; Rosenstock, H. M. *J. Chem. Phys.* **1964**, *41*, 3453.
(43) Small, G. J. *J. Chem. Phys.* **1971**, *54*, 3300.
(44) Mebel, A. M.; Hayashi, M.; Liang, K. K.; Lin, S. H. *J. Phys. Chem. A* **1999**, *103*, 10674.
(45) Sando, G. M.; Spears, K. G.; Hupp, J. T.; Ruhoff, P. T. *J. Phys. Chem.* **2001**, *105*, 5317.
(46) Sando, G. M.; Spears, K. G. *J. Phys. Chem.* **2001**, *105*, 5326.
(47) Seidner, L.; Domcke, W. *Chem. Phys.* **1994**, *186*, 27.
(48) Chuang, Y.; Truhlar, D. G. *J. Chem. Phys.* **2000**, *112*, 1221.
(49) Clary, D. C. *J. Chem. Phys.* **2001**, *114*, 9725.
(50) Leggett, A. J.; Chakravarty, S.; Dorsey, A. T.; Fisher, M. P.; Garg, A.; Zwerger, W. *Rev. Mod. Phys.* **1987**, *59*, 1.
(51) Lee, E.; Medvedev, E. S.; Stuchebrukhov, A. A. *J. Chem. Phys.* **2000**, *112*, 9015.
(52) Köppel, H.; Domcke, W.; Cederbaum, L. S. *Adv. Chem. Phys.* **1984**, *57*, 59.
(53) Duschinsky, F. *Acta Physicochim. (USSR)* **1937**, *7*, 551.
(54) Mebel, A. M.; Chen, Y.-T.; Lin, S.-H. *Chem. Phys. Lett.* **1996**, *258*, 53.
(55) Warshel, A.; Karplus, M. *Chem. Phys. Lett.* **1972**, *17*, 7.
(56) Warshel, A. *J. Chem. Phys.* **1975**, *62*, 214.
(57) Press, W. H.; Teukolsky, S. A.; Vetterling, W. T.; Flannery, B. P. *Numerical Recipes in C*, 2nd ed.; Cambridge University Press: Cambridge, U.K., 1992.
(58) Egorov, S. A.; Rabani, E.; Berne, B. J. *J. Chem. Phys.* **1997**, *108*, 1407.
(59) Sinclair, W. E.; Yu, H.; Phillips, D. *J. Chem. Phys.* **1997**, *106*, 5797.
(60) Kosloff, D.; Kosloff, R. *J. Comput. Phys.* **1983**, *52*, 35.
(61) Kosloff, R. *Annu. Rev. Phys. Chem.* **1994**, *45*, 145.
(62) Frisch, M. J.; Trucks, G. W.; Schlegel, H. B.; Scuseria, G. E.; Robb, M. A.; Cheeseman, J. R.; Zakrzewski, V. G.; Montgomery, J. A., Jr., Stratmann, R. E.; Burant, J. C.; Dapprich, S.; et al. *Gaussian 98*, Revision A.7; Gaussian, Inc.: Pittsburgh, PA, 1998.
(63) Scott, A.; Radom, L. *J. Phys. Chem.* **1996**, *100*, 16502.
(64) Ishida, T.; Rossky, P. J. *J. Phys. Chem. A* **2001**, *105*, 558.
(65) Ishida, T.; Rossky, P. J. To be submitted.
(66) Hwang, H.; Rossky, P. J. *J. Phys. Chem. A*, in press.
(67) Prezhdo, O.; Rossky, P. J. *Phys. Rev. Lett.* **1998**, *81*, 5294.
(68) Evans, D. G.; Coalson, R. *J. Chem. Phys.* **1992**, *97*, 5081.
(69) Cao, J.; Ungar, L. W.; Voth, G. A. *J. Chem. Phys.* **1996**, *104*, 4189.
(70) Kubo, R. *J. Phys. Soc. Jpn.* **1962**, *17*, 1100.
(71) Redfield, A. G. *Adv. Magn. Reson.* **1966**, *1*, 1.
(72) Schatz, G. C.; Ratner, M. A. *Quantum Mechanics in Chemistry*; Prentice-Hall: Englewood Cliffs, NJ, 1993.